JACS
JOURNAL OF THE AMERICAN CHEMICAL SOCIETY
Article
pubs.acs.org/JACS

Charge Transfer Structure–Reactivity Dependence of Fullerene–Single-Walled Carbon Nanotube Heterojunctions

Andrew J. Hilmer, Kevin Tvrdy, Jingqing Zhang, and Michael S. Strano*

Department of Chemical Engineering, Massachusetts Institute of Technology, Cambridge, Massachusetts 02139, United States

Supporting Information

ABSTRACT: Charge transfer at the interface between single-walled carbon nanotubes (SWCNTs) of distinct chiral vectors and fullerenes of various molecular weights is of interest both fundamentally and because of its importance in emerging photovoltaic and optoelectronic devices. One approach for generating isolated, discretized fullerene–SWCNT heterojunctions for spectroscopic investigation is to form an amphiphile, which is able to disperse the latter at the single-SWCNT level in aqueous solution. Herein, we synthesize a series of methanofullerene amphiphiles, including derivatives of C_{60}, C_{70}, and C_{84}, and investigated their electron transfer with SWCNT of specific chirality, generating a structure–reactivity relationship. In the cases of two fullerene derivatives, lipid–C_{61}–polyethylene glycol (PEG) and lipid–C_{71}–PEG, band gap dependent, incomplete quenching was observed across all SWCNT species, indicating that the driving force for electron transfer is small. This is further supported by a variant of Marcus theory, which predicts that the energy offsets between the nanotube conduction bands and the C_{61} and C_{71} LUMO levels are less than the exciton binding energy in SWCNT. In contrast, upon interfacing nanotubes with C_{85} methanofullerene, a complete quenching of all semiconducting SWCNT is observed. This enhancement in quenching efficiency is consistent with the deeper LUMO level of C_{85} methanofullerene in comparison with the smaller fullerene adducts, and suggests its promise as for SWCNT–fullerene heterojunctions.

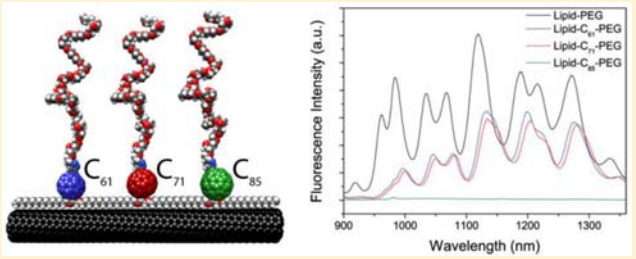

INTRODUCTION

Interfacing fullerenes with single-walled carbon nanotubes (SWCNTs) is desirable for a variety of applications, including carbon-based photovoltaics[1] and near-infrared fluorescence sensors.[2] Due to their resistance to photodamage[3] and high carrier mobilities, semiconducting SWCNTs hold great potential for utilization in near-infrared light harvesting photovoltaic devices. This is evidenced by emerging efforts in developing "all-carbon" photovoltaic active layers,[5−8] and it has recently been demonstrated that SWCNT-based photovoltaics outperform polymeric analogues in device lifetime measurements.[6] Although a large body of work has been directed at fabricating SWCNT-based devices, little work has been expended toward elucidating the kinetics of electron transfer at the SWCNT–fullerene interface, and these studies have focused on photoexcitation of fullerene, rather than SWCNT.[9,10] Such a study is beneficial, because a combination of factors, including morphology[6] and active-layer impurities,[5] can limit the quantum efficiency of photovoltaic devices. This is evidenced by the fact that the efficiencies of current, SWCNT-based active layer devices fall much lower than the theoretical value of 13%.[6] In addition, $PC_{60}BM$ is not an ideal electron acceptor for SWCNT-based photovoltaics because the LUMO level lies close to the SWCNT valence band, and therefore, the SWCNT–fullerene heterojunction has been predicted to switch from type II to type I upon increasing the SWCNT diameter of 0.9–1.3 nm.[6] The same is true of $PC_{70}BM$, due to similarity in electronic structure. However, C_{84} has a deeper LUMO level than that of C_{60} and C_{70},[11] as well as a higher photostability,[12] making it a potential candidate for SWCNT-based photovoltaics. Because of this, it is of interest to compare across different fullerenes and interfaces to develop structure–reactivity relationships for electron transfer in these systems, such that electron transfer can be optimized in the absence of complicating factors associated with device fabrication.

In addition to photovoltaic devices, SWCNT–fullerene junctions hold potential for utilization in SWCNT fluorescence-based sensors. SWCNT fluorescence-based sensors have demonstrated significant potential for the detection of a variety of small molecule analytes, including the direct detection of nitric oxide[13,14] and hydrogen peroxide,[15] as well as mediated detection of sugars[16] and adenosine triphosphate.[17] However, to observe molecular adsorption events, it is necessary that the adsorbing molecule possess redox properties which are capable of modulating the nanotube fluorescence.[2] For the detection of proteins and other biomacromolecules, which do not have redox properties, divalent ions such as Ni^{2+} near the nanotube surface have been utilized as an intermediate species in modulating nanotube fluorescence.[18] Fullerenes are expected to interact with SWCNT by accepting excited-state electrons from the SWCNT conduction band, thereby quenching the

Received: May 8, 2013
Published: July 15, 2013

   dx.doi.org/10.1021/ja404636b | J. Am. Chem. Soc. 2013, 135, 11901–11910

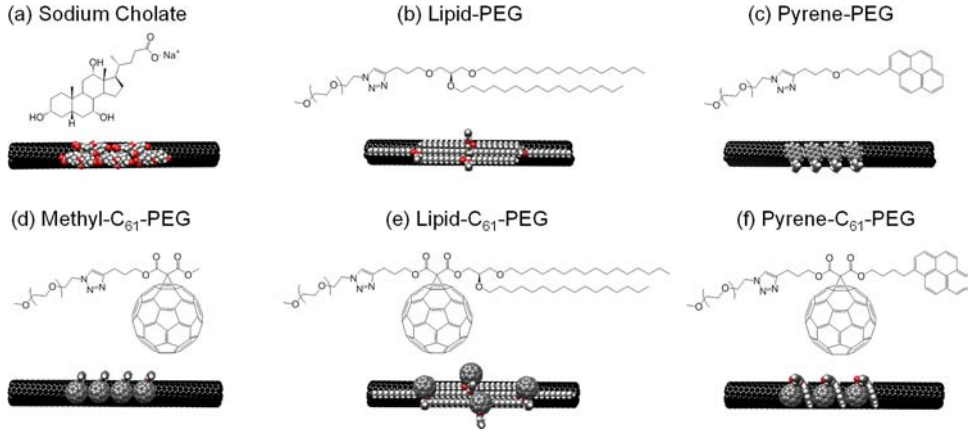

Figure 1. Surfactant systems utilized for analyzing interfacial effects on electron transfer, along with potential configurations on the SWCNT surface. In the molecular representations, PEG chains have been omitted for clarity. In these amphiphilic systems, the hydrophobic domains are expected to interact with the SWCNT surface, while the hydrophilic PEG chains extend into water.

SWCNT fluorescence signal. Because this process is distance dependent, it is possible that fullerenes could be employed as a distance dependent proximity quencher for transducing protein–SWCNT interactions in fluorescence-based SWCNT sensors.

In this study, we examine the interface between SWCNTs and fullerenes through the synthesis of a series of fullerene amphiphiles. These amphiphiles give stable suspensions of individual carbon nanotubes, thereby allowing for direct observation of the electronic interactions between these two species. The nature of the interface between the carbon nanotubes and fullerene molecules is probed by a solvatochromism model, and electron transfer characteristic are monitored by relative fluorescence quantum yields. We find that the relative fluorescence yields are dependent upon the fullerene species that is utilized, as well as the nature of the SWCNT–fullerene interface, and we are able to describe the electron transfer at these interfaces using a Marcus theory model.

EXPERIMENTAL SECTION

Nanotube Suspensions. HiPCO nanotubes (Unidym, Inc.) were initially suspended in 2% sodium cholate (SC). Nanotubes were dispersed at 1 mg of SWCNT/mL of 2% SC solution (~30 mL total volume) via 30 min of homogenization using a T-10 Ultra-Turrax (IKA Works, Inc.) dispersion element at approximately 11 400 min^{-1}. These dispersions were then sonicated in an ice bath at 10W for 1 h using a 6 mm probe tip (Cole-Parmer). Samples were subsequently centrifuged at 30 000 rpm (153 720 rcf) at 22 °C for 4 h, and the supernatant collected. 2% SC solutions were exchanged to the desired amphiphile by dialysis (3500 MWCO, Thermo Scientific). This pore size has previously been shown to remove sodium cholate while retaining the PEGylated surfactants.[19] For dialysis, equal volumes of 2% SC suspension (abs(625 nm) ~ 1.08) and amphiphile (2 mg/mL) were mixed, resulting in a final amphiphile concentration of 1 mg/mL. This suspension mixture was dialyzed against water for 4 days, with two water exchanges per day (V_{H_2O} > 200 × V_{SWCNT}), to ensure removal of sodium cholate.

Spectral Characterization. Photoluminescence spectra were acquired with a home-build, near infrared fluorescence microscope that has been described previously,[20] and an excitation wavelength of 785 nm. UV–vis–nIR absorbance measurements were carried out on a Shimadzu UV-310PC spectrometer.

RESULTS

Influence of SWCNT–Fullerene Interface. To study the influence of the fullerene–SWCNT interface on electron transfer, five surfactants were synthesized. These molecules were designed with hydrophobic domains, which preferentially adsorb to the SWCNT surface, and hydrophilic polyethylene glycol (PEG) chains (MW ~ 5000 Da), which extend into aqueous solution, imparting colloidal stability. Figure 1 shows potential configurations of the hydrophobic portions on the SWCNT surface. Here, PEG chains have been omitted for clarity. In designing these systems, we were particularly interested in studying how the nature of the SWCNT–fullerene interface influences the relative fluorescence yield of the SWCNT solution. Therefore, we synthesized molecules that would facilitate interfaces containing aliphatic (lipid–C_{61}–PEG) and polyaromatic (pyrene–C_{61}–PEG) domains, as well as a molecule that would facilitate direct contact between SWCNT and fullerene (methyl–C_{61}–PEG). As control molecules, lipid–PEG and pyrene–PEG surfactants were synthesized that lack the methanofullerene moiety. All nanotube suspensions were obtained by dialysis, starting from an initial, 2% sodium cholate nanotube suspension. In the case of the methyl-C_{61}–PEG derivative, visible aggregates were formed during the dialysis process, and bundles were observed by atomic force microscopy (AFM) (Figure S10, Supporting Information). Therefore, the results of the methyl-C_{61}–PEG suspensions are not discussed in the main body of this report. All other amphiphiles produced individually dispersed tubes, as evidenced by AFM (see Supporting Information), and the retention of large peak-to-valley ratios in the photoabsorbance spectra (Figure 2).

After surfactant exchange to the PEGylated amphiphiles, we attempted to remove the excess, free amphiphile by centrifugal filtration. For this purpose, 100 kDa MWCO centrifugal filters were unable to remove the excess macromolecules from solution, but 1000 kDa MWCO centrifugal filters proved successful at retaining SWCNTs while having enough porosity to pass the unbound amphiphiles (Figure S4, Supporting Information). However, the removal process resulted in visible aggregation in the case of pyrene–PEG and very slight changes in chirality distribution among the other suspensions, which likely resulted from small degrees of aggregation in the removal process. Therefore, all data presented in this report are for

SWCNT solutions that did not undergo this additional processing after dialysis.

UV−vis−nIR absorbance spectra for the initial sodium cholate suspension, as well as the four amphiphilic surfactant systems (without methyl-C_{61}−PEG) are shown in Figure 2. All suspensions have been diluted to similar concentrations and are plotted on the same scale. From visual inspection of these spectra, it is apparent that high peak-to-valley ratios are maintained during the exchange process, which is in agreement with the observation of individually dispersed tubes by AFM. In going from the lipid−PEG and pyrene−PEG control molecules to their methanofullerene analogues, a red shift in peak position is observed across all SWCNT species. In the case of pyrene−C_{61}−PEG, the red shift is greater than that observed in the case of the lipid−C_{61}−PEG derivative, indicating that there may be differences in the local dielectric environments in these two systems. This will be discussed in more detail later.

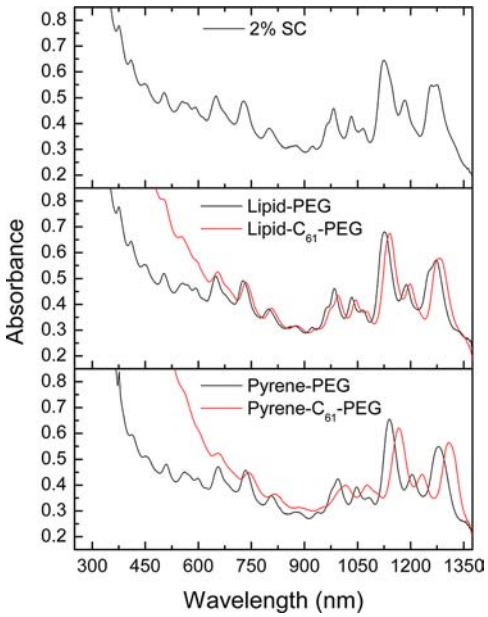

Figure 2. UV−vis−nIR absorbance spectra of five of the surfactant systems analyzed in this study (excluding methyl-C_{61}−PEG). The retention of high peak-to-valley ratios is indicative of high-quality SWCNT dispersions, in agreement with AFM observations of individually dispersed nanotubes.

Excitation−emission spectra for the lipid−PEG, lipid−C_{61}−PEG, pyrene−PEG, and pyrene−C_{61}−PEG suspensions are shown in Figure 3. In these plots, and in all fluorescence spectra presented in this report, the raw fluorescence intensities have been normalized using the baseline absorbance at the valley between approximately 900 and 925 nm to account for slight differences in nanotube concentrations across samples. As would be expected for a system in which electron transfer occurs between SWCNT and C_{61}, a quenching of nanotube fluorescence occurs upon incorporation of C_{61} into the surfactant structure. These plots also allowed for the determination of emission wavelengths for spectral deconvolution of fluorescence emission, as discussed in the next paragraph. To evaluate the extent to which each nanotube species is quenched by C_{61}, we sought to minimize the degree of C_{61} excitation by utilizing 785 nm excitation, where absorbance by the C_{61} moiety is minimal. This maximizes the likelihood of observing electron transfer from photoexcited SWCNT to C_{61}, while minimizing ground-state transfer from SWCNT to the photoexcited fullerene.

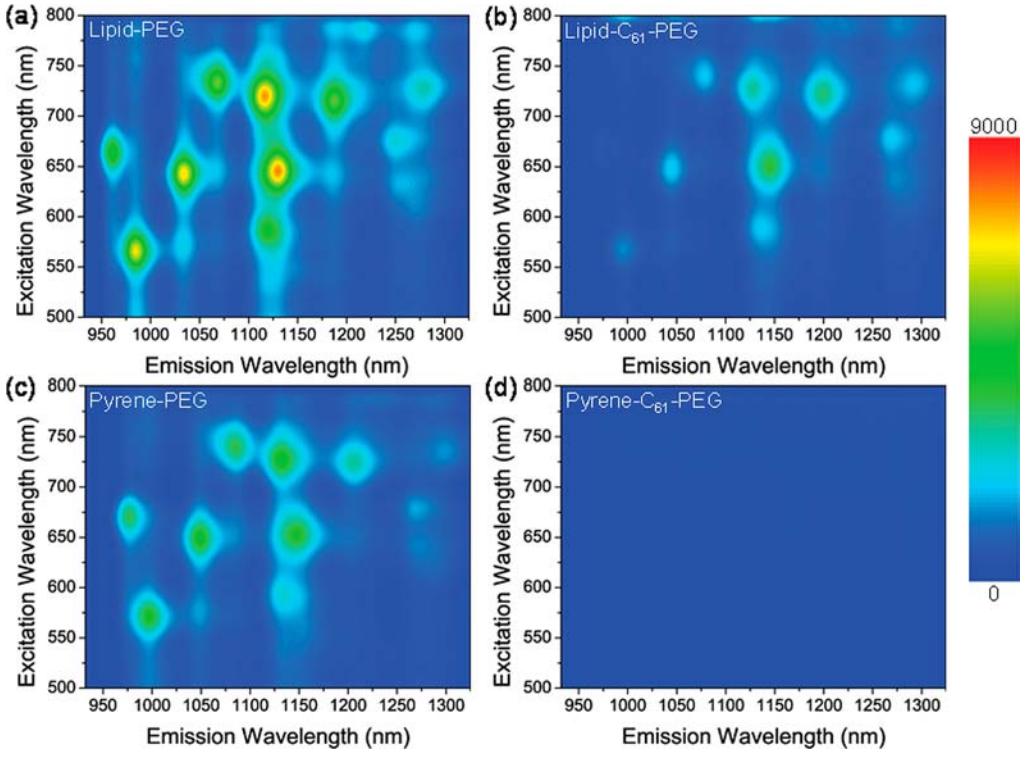

Figure 3. Excitation−emission plots for SWCNTs suspended in (a) lipid−PEG, (b) lipid−C_{61}−PEG, (c) pyrene−PEG, and (d) pyrene−C_{61}−PEG. All spectra are plotted on the same scale. All samples had similar SWCNT concentrations, and characteristic absorbance spectra for these samples are shown in Figure 1.

dx.doi.org/10.1021/ja404636b | J. Am. Chem. Soc. 2013, 135, 11901−11910

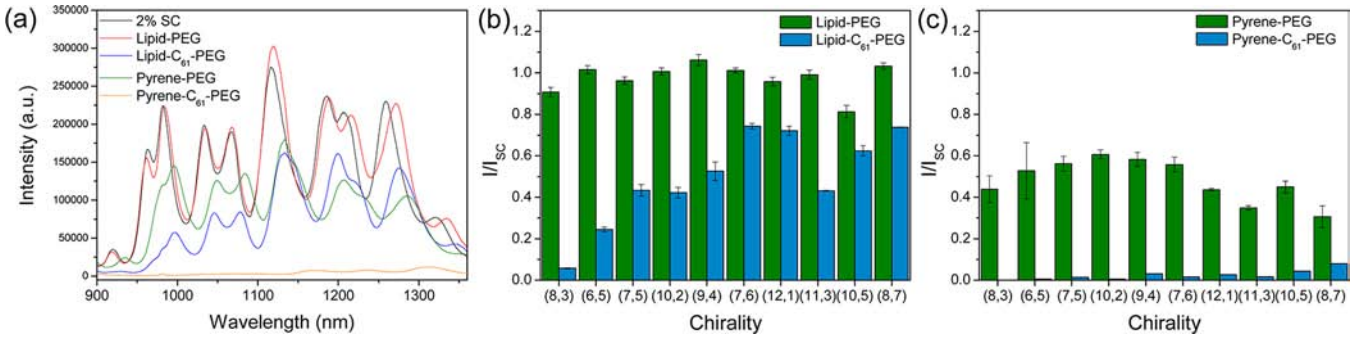

Figure 4. Fluorescence results for the surfactant systems analyzed in this study. (a) Fluorescence spectra of SWCNT suspensions, representing an average of three suspensions for each amphiphile (four samples for pyrene–PEG). (b) Fractional quenching results, relative to the intensity of SC–SWCNT, for the lipid–PEG and lipid–C_{61}–PEG systems. (c) Fractional quenching results, relative to SC–SWCNT, for the pyrene–PEG and pyrene–C_{61}–PEG systems.

Near-infrared fluorescence spectra, acquired with an excitation wavelength of 785 nm, are shown in Figure 4a. Using peak locations from the excitation–emission spectra in Figure 3, these spectra were further deconvoluted (see Supporting Information) into the emission contributions of 10 chiralities of carbon nanotubes, and the relative fluorescence intensities of these species, normalized to the fluorescence intensity of the initial sodium cholate solution, are presented in parts (b) and (c) of Figure 4. For the pyrene–C_{61}–PEG derivative, it was necessary to estimate peak positions due to the absence of clear fluorescence features in the excitation–emission spectra. In going from left to right, the nanotube chiralities are arranged from large to small band-gap, respectively. From Figure 4b, it is apparent that the lipid–PEG derivative produces solutions of similar fluorescence intensity as the initial sodium cholate solution, whereas in the case of lipid–C_{61}–PEG, a variable degree of quenching is observed for different SWCNT species, which appears to be band-gap dependent. For pyrene–PEG, a fluorescence quenching pattern is observed that does not have an apparent band-gap dependence. This quenching is substantially enhanced on the addition of the methanofullerene moiety, resulting in near-complete quenching of the fluorescence across all species.

Fullerene Family Analysis. In addition to analyzing the influence of the fullerene–SWCNT interface on the relative fluorescence quantum yield, we synthesized two additional lipid–fullerene amphiphiles based on C_{71} and C_{85} methanofullerenes (Figure 5). Using these species, we sought to investigate how the SWCNT quantum yield is influenced by the energy states of the fullerene derivative.

Excitation–emission spectra for the C_{71} and C_{85} fullerene systems are shown in Figure 6. Here it is apparent that, like the C_{61} derivative, the C_{71} moiety produces incomplete fluorescence quenching across all species. In contrast, the introduction of C_{85} to the surfactant results in complete fluorescence quenching across all species. Absorbance and fluorescence spectra for the three lipidic methanofullerene derivatives are presented in Figure 7. In the cases of the C_{61} and C_{71} surfactant systems, the onset of absorbance below 715 nm is attributable to the methanofullerene moieties, with C_{71} exhibiting a stronger absorbance in the visible region.[21] In the case of the C_{85} methanofullerene, the fullerene absorbance extends into the nIR region, accounting for the apparent increase in the sample baseline. In addition, the C_{85} sample exhibits a higher degree of peak broadening compared to the other methanofullerene species, which we attribute to inhomogeneous broadening that results from the presence of multiple isomers of C_{85} monoadducts. The fluorescence spectra in Figure 7b, acquired at an excitation wavelength of 785 nm, show similar degrees of quenching for the C_{61} and C_{71} methanofullerenes, but a complete quenching of nanotube fluorescence across all species in the case of the C_{85} adduct. These results are shown more quantitatively in the deconvoluted relative intensities, which are presented in Figure 7c.

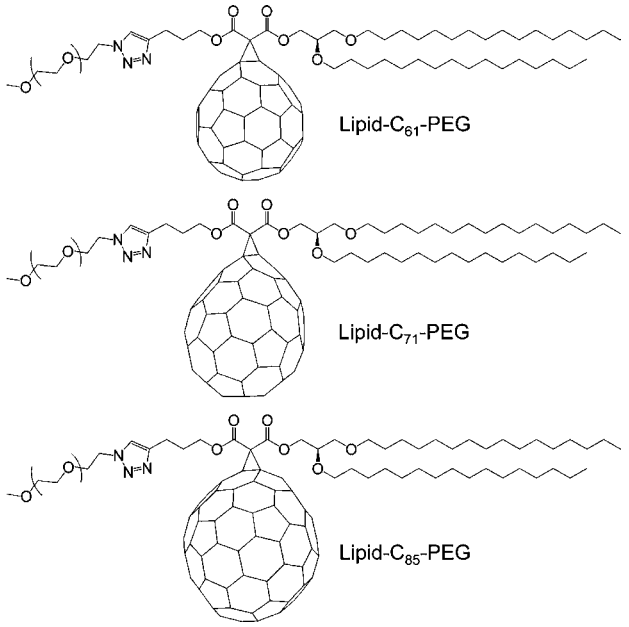

Figure 5. Fullerene family analysis. From top to bottom, methanofullerenes based on C_{60}, C_{70}, and C_{84}, respectively.

DISCUSSION

Evaluating the Composition of the Adsorbed Layer. To better understand the observed differences in fluorescence quenching for the various amphiphilic systems in Figures 4 and 7, we sought to first quantify the composition of the adsorbed layer in these systems. In an aqueous surfactant system, SWCNTs that are exposed to water can be quenched by a variety of mechanisms, including sidewall protonation,[22] or interaction with oxygen[23] and reactive oxygen species.[15,24] Therefore, we sought to quantify the percentage of the

dx.doi.org/10.1021/ja404636b | J. Am. Chem. Soc. 2013, 135, 11901–11910

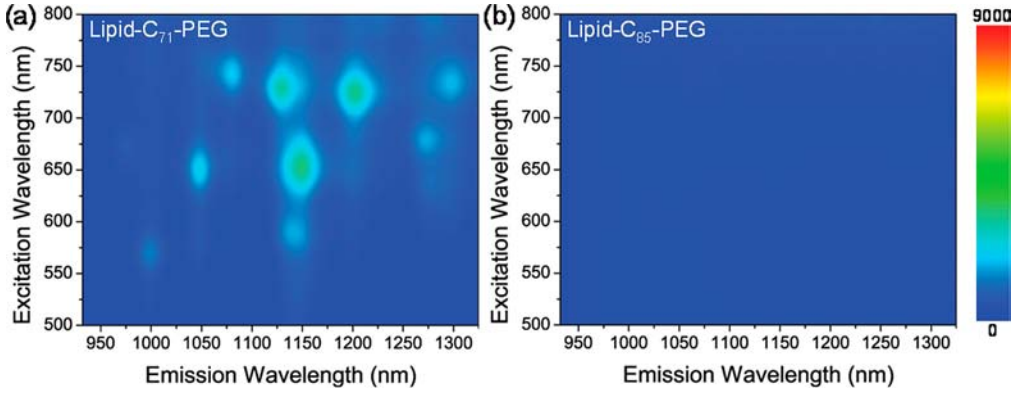

Figure 6. Excitation−emission plots for SWCNTs suspended in (a) lipid−C_{71}−PEG and (b) lipid−C_{85}−PEG. Spectra are plotted on the same scale as in Figure 3. All samples had similar SWCNT concentrations, and characteristic absorbance spectra for these samples are shown in Figure 7.

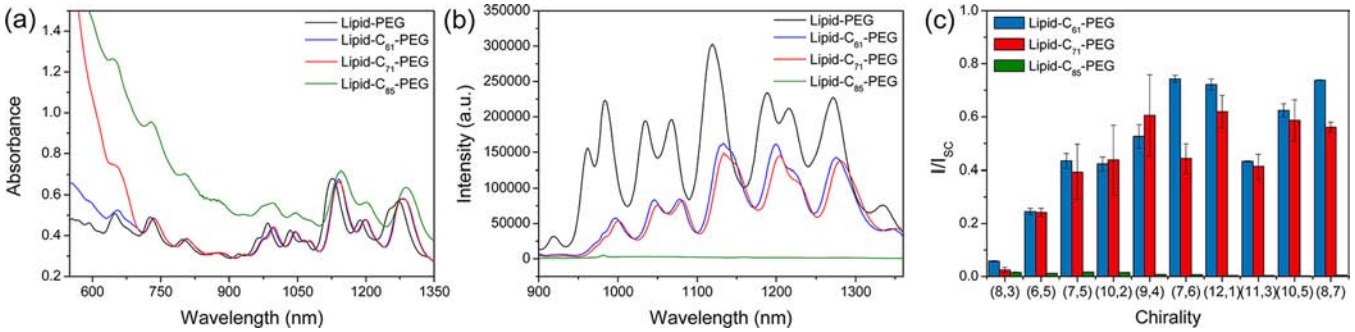

Figure 7. Absorbance and fluorescence results from fullerene family analysis. (a) Characteristic absorbance spectra of SWCNT suspensions in lipid−PEG, lipid−C_{61}−PEG, lipid−C_{71}−PEG, and lipid−C_{85}−PEG. (b) Averaged fluorescence spectra (three samples) for these amphiphilic systems, acquired at an excitation wavelength of 785 nm. (c) Deconvoluted relative intensities, normalized by the intensities of SC-SWCNTs, for the three lipidic methanofullerenes.

SWCNT surface that is exposed to water to determine the role of the aqueous environment in the observed, fluorescence quenching behavior.

It has previously been shown that the solvatochromic shifts of the SWCNT optical transitions are dependent upon the local SWCNT dielectric environment by the following relation[25]

$$\Delta E_{ii} = -L\frac{\Delta\alpha_{ii}}{R^3}\left[\frac{2(\varepsilon - 1)}{2\varepsilon + 1} - \frac{2(n^2 - 1)}{2n^2 + 1}\right]$$

where L is a fluctuation factor, ε is the local dielectric constant, n is the refractive index, R is the nanotube radius, and $\Delta\alpha_{ii}$ is the change in polarizability of SWCNTs upon excitation from the ground to excited state. Choi et al.[25] have shown that this difference in polarizability is predominantly determined by the longitudinal polarizability of the exciton, allowing for $\Delta\alpha_{ii}$ to be approximated by $\alpha_{ii_{\parallel}}$. Using a longitudinal polarizability of the form $\alpha_{ii} \propto 1/(RE_{ii}^2)$, the following equation is obtained:[25]

$$(E_{ii})^2\Delta E_{ii} = -K\left[\frac{2(\varepsilon - 1)}{2\varepsilon + 1} - \frac{2(n^2 - 1)}{2n^2 + 1}\right]\left(\frac{1}{R^4}\right) = \frac{c}{R^4}$$

To quantify the surfactant surface coverage, it is necessary to utilize a single-component system, with a known dielectric constant and refractive index as a reference. We utilized *N*-methyl-2-pyrrolidone (NMP) as a reference system, which has a dielectric constant of 32.2 and a refractive index of 1.47. From Choi et al.[25] we know that for NMP, the plot of $(E_{11})^2\Delta E_{11}$ vs $1/d^4$ gives a slope of c = 0.060 eV^3 nm^4.

Using this reference system, we first analyzed the surface coverage in the lipid−PEG and pyrene−PEG suspensions. From the excitation−emission maps of the lipid−PEG and pyrene−PEG dispersions, we plotted $(E_{11})^2\Delta E_{11}$ vs $1/d^4$ to obtain a slopes of 0.0517 and 0.0619 eV^3 nm^4, respectively (Figure 8). Using these values, along with prior experimental results for NMP, it was possible to evaluate the local dielectric constant of the lipid−PEG (pyrene−PEG) SWCNT system using the following relation:

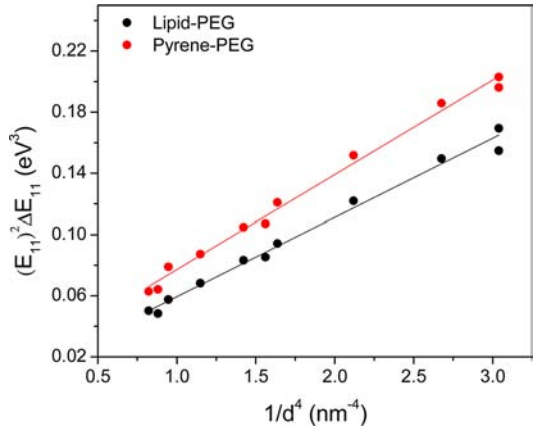

Figure 8. Plots of $(E_{11})^2\Delta E_{11}$ versus $1/d^4$, evaluated from excitation−emission plots, for lipid−PEG and pyrene−PEG suspensions. The slopes of these curves were used to quantify the SWCNT surface area that is exposed to the aqueous environment.

dx.doi.org/10.1021/ja404636b | J. Am. Chem. Soc. 2013, 135, 11901−11910

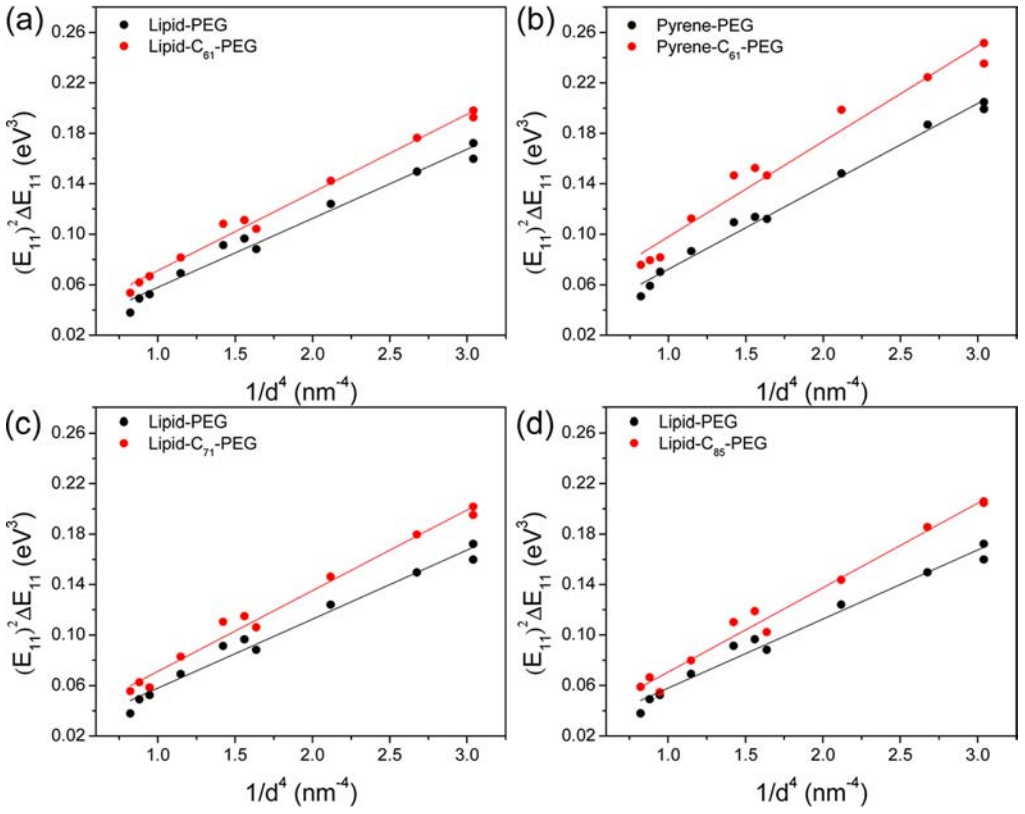

Figure 9. Plots of $(E_{11})^2\Delta E^{11}$ versus $1/d^4$ evaluated by deconvoluting absorbance spectra for all four fullerene surfactants. Each amphiphilic fullerene system is compared with its fullerene-free control molecule. (a) lipid−C_{61}−PEG; (b) pyrene−C_{61}−PEG; (c) lipid−C_{71}−PEG; (d) lipid−C_{85}−PEG. The slopes of these curves were used to quantify the SWCNT surface area that is exposed to the aqueous environment.

$$\frac{c_2}{c_1} = \frac{\left(\frac{2(\varepsilon_2 - 1)}{2\varepsilon_2 + 1} - \frac{2(n_2^2 - 1)}{2n_2^2 + 1}\right)}{\left(\frac{2(\varepsilon_1 - 1)}{2\varepsilon_1 + 1} - \frac{2(n_1^2 - 1)}{2n_1^2 + 1}\right)}$$

Here, subscripts 1 and 2 refer to properties associated with the NMP and lipid−PEG (pyrene−PEG) systems, respectively, and it has been assumed that K is invariant across SWCNT solutions. Solving this equation, and assuming that the refractive index of the surfactant-dispersed SWCNTs is equal to that of water (1.333), we obtained local dielectric constants of 6.56 for the lipid−PEG suspension and 11.56 for the pyrene−PEG suspension. Assuming that the local dielectric constant in the lipid−PEG system is composed of contributions from the lipid segment and water

$$\bar{\varepsilon} = x_1\varepsilon_{\text{lipid}} + (1 - x_1)\varepsilon_{H_2O}$$

it is possible to evaluate the surface coverage of the lipid molecule on the SWCNT surface. Here, the surface coverage of a particular component is defined as x_i, or the fractional contribution of that component to the overall, local dielectric constant at the nanotube surface. For the lipidic segment, we assumed a dielectric constant of 2.08, which corresponds to that of hexadecane,[26] and the dielectric constant of water was taken to be 80.1. Using these values in the above expression gave a 94.3% surface coverage of the lipidic moiety, corresponding to a 5.7% surface coverage of water. These values are very close to the recently estimated surfactant surface coverage for sodium cholate suspended SWCNTs of 93 ± 15%,[27] explaining the similarity in fluorescence intensity for these two systems. For the pyrene−PEG system, $\varepsilon_{\text{pyrene}}$ was taken to be 3.19, which is the average of the three primary tensor components in pyrene crystals.[28] Using this value, the surface coverages of pyrene and water were determined to be 89.1 and 10.9%, respectively. In this system, the similarity in water surface coverage to that of sodium cholate indicates that the pyrene moiety appears to be responsible for partial quenching of the SWCNT fluorescence.

Due to the fact that the lipid−C_{85}−PEG and pyrene−C_{61}−PEG systems have complete or near-complete quenching of the SWCNT fluorescence, we then utilized the local dielectric constant of the lipid−PEG system as a reference and used solvatochromic shifts in the absorbance spectra (as opposed to fluorescence spectra) to deduce information about the surface coverage of water in each fullerene-based amphiphilic system. Plots of $(E_{11})^2\Delta E_{11}$ vs $1/d^4$, obtained by deconvoluting absorbance data, are provided in Figure 9 for the four fullerene surfactant systems. Overlayed plots of $(E_{11})^2\Delta E_{11}$ vs $1/d^4$, evaluated from absorbance and fluorescence spectra, showed good agreement between methods and are provided in Figure S3 of the Supporting Information. Because there are three components in all of the fullerene surfactant systems, lipid−C_{61}−PEG, lipid−C_{71}−PEG, lipid−C_{85}−PEG, and pyrene−C_{61}−PEG, we were unable to solve for each of the components directly but were able to bound the quantity of water on the surface, due to its high static dielectric constant. For example, for the lipid−C_{61}−PEG system, in which the local dielectric constant is specified by

$$\bar{\varepsilon} = x_1\varepsilon_{\text{lipid}} + x_2\varepsilon_{C_{60}} + (1 - x_1 - x_2)\varepsilon_{H_2O}$$

we sequentially set x_1 and x_2 to zero and then solved for the coverage of the other two components. In performing the

dx.doi.org/10.1021/ja404636b | J. Am. Chem. Soc. 2013, 135, 11901−11910

analysis, the dielectric constants of C_{61}, C_{71}, and C_{85} were taken to be 3.6,[29] 3.8,[30] and 5.5,[31] respectively.

The resulting bounds for the surface coverage of water, in each surfactant system, are given in Table 1. For systems in which it was possible to evaluate surface coverages by both absorbance and fluorescence methods, a comparison of results is provided in Table S1 of the Supporting Information. Again, predicted surface coverage values fall within a few percent of each other, indicating good agreement between the two methods. The results in Table 1 indicate a similar coverage of water in the cases of lipid−C_{61}−PEG, lipid−C_{71}−PEG, and lipid−C_{85}−PEG, suggesting that exposure to the aqueous environment cannot be responsible for the differences in fluorescence quenching observed among these surfactant systems. In comparing the C_{61} derivatives, the pyrene−C_{61}−PEG suspension is predicted to have a much higher surface coverage of water than that of the lipid−C_{61}−PEG system. Therefore, we expect that a combination of factors, including the pyrene and fullerene moieties, as well as increased exposure to the aqueous environment, are responsible for the increased fluorescence quenching of this system relative to that of lipid−C_{61}−PEG.

Table 1. Quantifying Exposed Surface Area

Surfactant System	Estimated Water Coverage
2% sodium cholate	7 ± 15%[a]
lipid−PEG	5.7%
pyrene−PEG	10.9%
lipid−C_{61}−PEG	7.4−9.3%
pyrene−C_{61}−PEG	40.4−40.7%
lipid−C_{71}−PEG	8.8−10.8%
lipid−C_{85}−PEG	9.8−13.7%

[a]In ref.27

This analysis helps to explain differences in fluorescence quenching between the pyrene−C_{61}−PEG and lipid−C_{61}−PEG systems but fails to explain the differences in fluorescence quenching between the C_{61}, C_{71}, and C_{85} derivatives. In addition, it cannot account for the apparent, band-gap dependent quenching of the nanotube fluorescence in the C_{61} and C_{71} systems. We hypothesized that these trends could be due to differences in electron transfer energetics, which are expected to vary as a function of both the electron acceptor and the chirality of the carbon nanotubes. Therefore, to explain these trends, we attempted to model the experimental data using Marcus theory.

Analysis of Electron Transfer Energetics. To verify that electron transfer is responsible for SWCNT fluorescence quenching, we attempted to fit the lipid−C_{61}−PEG and lipid−C_{71}−PEG fluorescence data using a Marcus theory model. Due to the incomplete fluorescence quenching in the cases of the lipid−C_{61}−PEG and lipid−C_{71}−PEG derivatives, it was possible to utilize the relative degrees of quenching to infer information about the relative rates of electron transfer between excited-state SWCNTs and fullerenes. This is because, among competing excited-state decay pathways in SWCNT, the selectivity toward a particular pathway, in this case electron transfer to fullerene, will be proportional to the rate constant associated with that pathway. Because energy transfer ultimately diverts an electron from the radiative decay pathway, fractional quenching results can be utilized as an approximation for the rate constant of electron transfer. If the fractional quenching is normalized to a particular chirality, such as (6,5), it is possible to approximate relative rate constants for electron transfer as

$$\left(\frac{k_{et}^{(n,m)}}{k_{et}^{(6,5)}}\right)_{expt} = \frac{1-(I/I_o)_{(n,m)}}{1-(I/I_o)_{(6,5)}}$$

According to Marcus theory, the rate constant associated with electron transfer from SWCNT to the LUMO level of fullerene can be represented as:[32]

$$k_{et} = \frac{2\pi}{\hbar\sqrt{4\pi\lambda k_b T}} V_R{}^2 \exp(-\Delta G_{(n,m)}{}^{\ddagger}/kT)$$

$$= \frac{2\pi}{\hbar\sqrt{4\pi\lambda k_b T}} V_R{}^2 \exp\left(-\frac{(\lambda + \Delta G_{(n,m)}{}^{o})^2}{4\lambda kT}\right)$$

Here, $V_R{}^2$ is an electronic coupling term between the initial and final states, λ is the reorganization energy, and $\Delta G_{(n,m)}{}^{o}$ is total change in Gibbs free energy for the electron transfer event. The change in Gibbs free energy is related to the energy difference between the SWCNT conduction band and the LUMO level of the methanofullerene by the following relation:

$$\Delta G_{(n,m)}{}^{o} = -(E_{(n,m)}{}^{c} - E^{LUMO})$$

Table 2. Predicted Donor−Acceptor Energy Offsets for Different Fullerenes and Reorganization Energies

			Energy Offset, $-\Delta G_o$ (eV)					
			C_{61}		C_{71}		C_{85}[c]	
Chirality	$E_c^{(n,m)}$[a]	$E_b^{(n,m)}$[b]	$E_{\lambda=0.23}^{LUMO} = -3.95$	$E_{\lambda=0.51}^{LUMO} = -4.05$	$E_{\lambda=0.23}^{LUMO} = -4.00$	$E_{\lambda=0.51}^{LUMO} = -4.14$	$E_{\lambda=0.23}^{LUMO} = -4.30$	$E_{\lambda=0.51}^{LUMO} = -4.40$
(8,3)	−3.83	0.38	0.12	0.22	0.17	0.31	0.47	0.57
(6,5)	−3.85	0.40	0.10	0.20	0.15	0.29	0.45	0.55
(7,5)	−3.86	0.36	0.09	0.19	0.14	0.28	0.44	0.54
(10,2)	−3.86	0.34	0.09	0.19	0.14	0.28	0.44	0.54
(9,4)	−3.90	0.33	0.05	0.15	0.10	0.24	0.40	0.50
(7,6)	−3.90	0.34	0.05	0.15	0.10	0.24	0.40	0.50
(12,1)	−3.93	0.30	0.02	0.12	0.07	0.21	0.37	0.47
(11,3)	−3.90	0.30	0.05	0.15	0.10	0.24	0.40	0.50
(10,5)	−3.91	0.29	0.04	0.14	0.09	0.23	0.39	0.49
(8,7)	−3.91	0.29	0.04	0.14	0.09	0.23	0.39	0.49

[a]E_c values were utilized from Tanaka et al.[33] [b]The exciton binding energy of SWCNTs was approximated by $E_b = 0.3/d_t$ where d_t is the diameter of the nanotube.[44] [c]LUMO levels of C_{85} were approximated by assuming a 0.35 eV energy offset relative to C_{61}.[11]

dx.doi.org/10.1021/ja404636b | J. Am. Chem. Soc. 2013, 135, 11901−11910

If we assume that the electronic coupling term is invariant across nanotube species, relative rate constants of electron transfer can be evaluated, allowing for direct comparison with experimental fractional quenching results:

$$\left(\frac{k_{et}^{(n,m)}}{k_{et}^{(6,5)}}\right)_{theory} = \frac{\exp(-\Delta G_{(n,m)}^{\ddagger}/kT)}{\exp(-\Delta G_{(6,5)}^{\ddagger}/kT)}$$

This relative rate equation is only dependent upon the reorganization energy of electron transfer and the energy offsets between the fullerene LUMO and the SWCNT conduction bands. SWCNT conduction band energies, referenced to the standard hydrogen electrode (SHE), have been reported in the literature for several chiralities.[33] These values were converted to absolute potential using the relation $E_{abs}(V) = -(E_{SHE}(V) + 4.44\ V)$[34] and are reported in the second column of Table 2. Additionally, reorganization energies for fullerene-based electron transfer systems have been reported to be from 0.23 to 0.77 eV.[35−38] Here, we sought to bound the energy offset $\Delta G_{(n,m)}$°between SWCNTs and the fullerenes in this study using the Marcus theory equation above. To do so, we utilized a reorganization energy of 0.23 eV as a lower limit, with an upper limit of 0.51 eV, which has specifically been observed for fullerene-based dyads with short donor−acceptor linkages.[35] Using experimental fractional quenching results, we then fit the effective fullerene LUMO level, E^{LUMO}, thereby allowing for determination of $\Delta G_{(n,m)}$°. The fitted LUMO levels for C_{61} and C_{71} are provided in Table 2 for assumed reorganization energies of both 0.23 and 0.51. The LUMO level of C_{85} was then deduced from the LUMO level of C_{61} by assuming that the LUMO level of C_{85} is 0.35 eV lower than that of C_{61}.[11]

From the values in Table 2, is it evident that the obtained LUMO levels for C_{61} (−3.95 to −4.05 eV) deviate slightly from the values of −1.028 to −1.08 V vs Fc/Fc+ or approximately −3.85 to −3.8 eV (using the conversion (LUMO = -e(4.88 V + $E_{red}^{Fc/Fc+}$))[39]) that have been previously reported for C_{60} monoadducts.[11,40,41] However, as shown in Figure 10, the fitted LUMO levels result in SWCNT−fullerene energy offsets ($\Delta G_{(n,m)}^{o}$) that are in good agreement with ab initio results, which incorporate polarization effects at the SWCNT−fullerene interface.[6] Therefore, we anticipate that electronic interactions are also responsible for the deviation in the current case. Experimentally, near-identical LUMO levels to C_{61} have been observed for C_{71},[11,41] due to the similarity in electronic properties of these two fullerenes,[42] and this is consistent with the similarity in offsets that result from our model.

In organic photovoltaics, it is generally accepted that LUMO−LUMO offsets greater than the exciton binding energy are necessary to enable efficient interfacial energy transfer.[43] As shown in Figure 10, in the case of the C_{61} and C_{71} derivatives, both systems possess energy offsets that fall below the exciton binding energy of SWCNTs, which was approximated by $E_b = b/d_t$ where b = 0.3 eV·nm.[44] This is likely the reason for the inefficient fluorescence quenching of the nanotubes in these two systems. In contrast, the deeper LUMO level of C_{85} produces energy offsets greater than the exciton binding energy, resulting in energetically favorable electron transfer, and complete fluorescence quenching across all nanotube species. However, the results for the C_{85} derivative are complicated by the fact that this fullerene adduct has an absorbance component that extends beyond 785 nm, which is the excitation wavelength utilized in this study. Therefore, follow-up work on the dynamics of this interface will provide greater insight into the electronic coupling between these species.

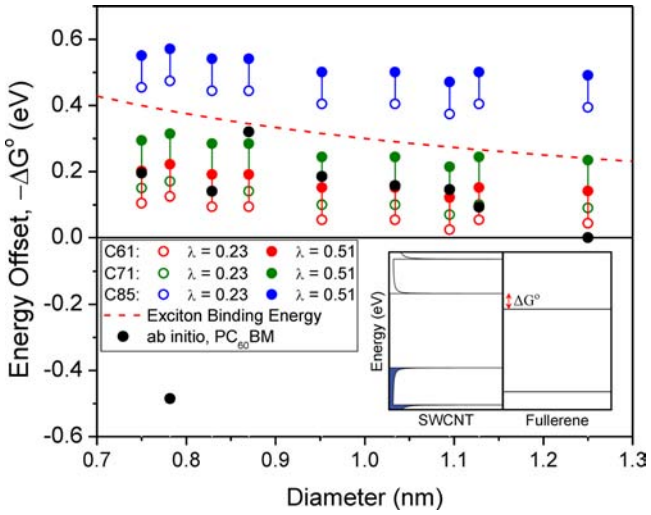

Figure 10. Predicted energy offsets between SWCNT conduction bands and fullerene LUMO levels. Offsets for C_{61} and C_{71} were determined by fitting Marcus theory to experimental data. Offsets for C_{85} were estimated by assuming a C_{85} LUMO level that is 0.35eV lower than that of C_{61}.[11] The data are compared with ab initio values reported in ref 6 for $PC_{61}BM$. The general trend for the binding energy was evaluated using E_b (eV) = 0.3/d_t.[44]

To validate the application of the Marcus theory model in this study, we plotted the experimentally determined relative rate constants of electron transfer vs those predicted by the Marcus theory model. The resulting parity plot is presented in Figure 11, and a direct comparison of experimental and theoretical values is provided in Table 3. Deviations of data points from a one-to-one parity relationship may result from limitations in the usage of relative fluorescence quenching as an approximation for relative rate constants of electron transfer, because certain nanotube chiralities may experience small differences in their local environments, or slight redistributions in nanotube chirality may occur during the dialysis procedure. These factors can cause slight changes in fluorescence quenching, which are not attributable to excited-state electron transfer. However, as can be seen from the plot, good

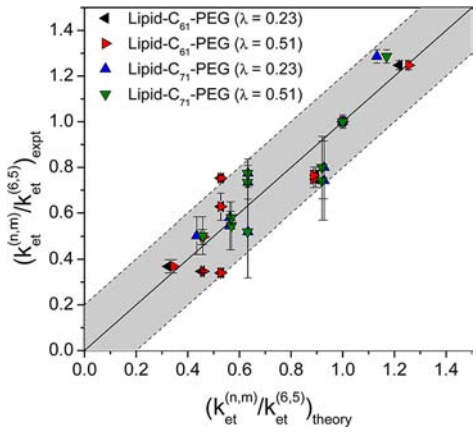

Figure 11. Parity plot showing the agreement between experimental and theoretical relative rate constants for different values of the reorganization energy.

dx.doi.org/10.1021/ja404636b | J. Am. Chem. Soc. 2013, 135, 11901−11910

Table 3. Comparison between Experimental and Theoretical Relative Rate Constants of Electron Transfer

		Summary of Relative Rate Constant Results, $k_{ET}^{(n,m)}/k_{ET}^{(6,5)}$					
		C_{61}			C_{71}		
			Marcus theory			Marcus theory	
Chirality	Diameter (nm)	Experimental	$E_{\lambda=0.23}^{LUMO} = -3.95$	$E_{\lambda=0.51}^{LUMO} = -4.05$	Experimental	$E_{\lambda=0.23}^{LUMO} = -4.00$	$E_{\lambda=0.51}^{LUMO} = -4.14$
(8,3)	0.782	1.25 ± 0.02	1.22	1.26	1.29 ± 0.02	1.13	1.17
(6,5)	0.757	1.00 ± 0.02	1.00	1.00	1.00 ± 0.03	1.00	1.00
(7,5)	0.829	0.75 ± 0.05	0.90	0.89	0.80 ± 0.17	0.93	0.92
(10,2)	0.884	0.77 ± 0.05	0.90	0.89	0.74 ± 0.23	0.93	0.92
(9,4)	0.916	0.63 ± 0.09	0.53	0.53	0.52 ± 0.39	0.63	0.63
(7,6)	0.895	0.34 ± 0.05	0.53	0.53	0.73 ± 0.10	0.63	0.63
(12,1)	0.995	0.37 ± 0.08	0.32	0.34	0.50 ± 0.16	0.43	0.46
(11,3)	1.014	0.75 ± 0.02	0.53	0.53	0.77 ± 0.08	0.63	0.63
(10,5)	1.050	0.50 ± 0.07	0.45	0.46	0.55 ± 0.19	0.56	0.57
(8,7)	1.032	0.35 ± 0.02	0.45	0.46	0.58 ± 0.05	0.56	0.57

agreement is observed between experimental and theoretical results.

CONCLUSIONS

To examine electron transfer at the interface between SWCNTs and fullerenes, we synthesized a series of methanofullerene surfactants. For all amphiphiles studied here, with the exception of the methyl-C_{61}–PEG derivative, high-quality dispersions of individual nanotubes were obtained upon surfactant exchange from 2% sodium cholate. In the cases of lipid–C_{61}–PEG and lipid–C_{71}–PEG, which are predicted to have similar surfactant surface coverages, band-gap dependent, incomplete quenching was observed across all semiconducting species. In the case of pyrene–C_{61}–PEG, near-complete quenching of SWCNT fluorescence was observed, which is attributed to partial quenching by both the pyrene and fullerene moieties, as well as significant exposure of the SWCNT surface to the aqueous environment. The incomplete quenching in the cases of lipid–C_{61}–PEG and lipid–C_{71}–PEG indicates that the driving force for excited-state electron transfer is small in these systems. This is further supported by a Marcus theory model, which predicts that the energy offsets between the SWCNT conduction bands and the fullerene LUMO levels are less than the SWCNT exciton binding energy. In contrast, the lipid–C_{85}–PEG derivative shows complete quenching of all SWCNT species utilized in this work. This enhancement in quenching efficiency is consistent with the fact that the LUMO level of C_{85} methanofullerene is approximately 0.35 eV lower than that of the smaller fullerene adducts, resulting in energy offsets that exceed the exciton binding energy. This result, combined with the fact that C_{85} has much higher photostability than that of C_{61} and C_{71}, makes this larger fullerene adduct a promising candidate for SWCNT-based sensors and photovoltaics.

ASSOCIATED CONTENT

Supporting Information

Synthetic protocols, solvatochromism data, absorbance spectra, and AFM images, details of spectral deconvolution, and MALDI-TOF and 1H NMR spectra. This material is available free of charge via the Internet at http://pubs.acs.org.

AUTHOR INFORMATION

Corresponding Author

strano@mit.edu

Notes

The authors declare no competing financial interest.

ACKNOWLEDGMENTS

This research is supported in part by the Department of Energy Office of Science Graduate Fellowship Program (DOE SCGF), made possible in part by the American Recovery and Reinvestment Act of 2009, administered by ORISE-ORAU under contract no. DE-AC05-06OR23100.

REFERENCES

(1) Dai, L. M.; Chang, D. W.; Baek, J. B.; Lu, W. *Small* **2012**, *8*, 1130.
(2) Boghossian, A. A.; Zhang, J. Q.; Barone, P. W.; Reuel, N. F.; Kim, J. H.; Heller, D. A.; Ahn, J. H.; Hilmer, A. J.; Rwei, A.; Arkalgud, J. R.; Zhang, C. T.; Strano, M. S. *ChemSuschem* **2011**, *4*, 848.
(3) Barone, P. W.; Parker, R. S.; Strano, M. S. *Anal. Chem.* **2005**, *77*, 7556.
(4) Durkop, T.; Getty, S. A.; Cobas, E.; Fuhrer, M. S. *Nano Lett.* **2004**, *4*, 35.
(5) Jain, R. M.; Howden, R.; Tvrdy, K.; Shimizu, S.; Hilmer, A. J.; McNicholas, T. P.; Gleason, K. K.; Strano, M. S. *Adv. Mater.* **2012**, *24*, 4436.
(6) Bernardi, M.; Lohrman, J.; Kumar, P. V.; Kirkeminde, A.; Ferralis, N.; Grossman, J. C.; Ren, S. *ACS Nano* **2012**, *6*, 8896.
(7) Ramuz, M. P.; Vosgueritchian, M.; Wei, P.; Wang, C.; Gao, Y.; Wu, Y.; Chen, Y.; Bao, Z. *ACS Nano* **2012**, *6*, 10384.
(8) Bindl, D. J.; Arnold, M. S. *J. Phys. Chem. C* **2013**, *117*, 2390.
(9) Sandanayaka, A. S. D.; Maligaspe, E.; Hasobe, T.; Ito, O.; D'Souza, F. *Chem. Commun.* **2010**, *46*, 8749.
(10) D'Souza, F.; Chitta, R.; Sandanayaka, A. S. D.; Subbaiyan, N. K.; D'Souza, L.; Araki, Y.; Ito, O. *J. Am. Chem. Soc.* **2007**, *129*, 15865.
(11) Kooistra, F. B.; Mihailetchi, V. D.; Popescu, L. M.; Kronholm, D.; Blom, P. W. M.; Hummelen, J. C. *Chem. Mater.* **2006**, *18*, 3068.
(12) Juha, L.; Ehrenberg, B.; Couris, S.; Koudoumas, E.; Leach, S.; Hamplova, V.; Pokorna, Z.; Mullerova, A.; Kubat, P. *Chem. Phys. Lett.* **2001**, *335*, 539.
(13) Zhang, J.; Boghossian, A. A.; Barone, P. W.; Rwei, A.; Kim, J.-H.; Lin, D.; Heller, D. A.; Hilmer, A. J.; Nair, N.; Reuel, N. F.; Strano, M. S. *J. Am. Chem. Soc.* **2010**, *133*, 567.
(14) Kim, J. H.; Heller, D. A.; Jin, H.; Barone, P. W.; Song, C.; Zhang, J.; Trudel, L. J.; Wogan, G. N.; Tannenbaum, S. R.; Strano, M. S. *Nat. Chem.* **2009**, *1*, 473.
(15) Jin, H.; Heller, D. A.; Kalbacova, M.; Kim, J. H.; Zhang, J. Q.; Boghossian, A. A.; Maheshri, N.; Strano, M. S. *Nat. Nanotechnol.* **2010**, *5*, 302.
(16) Mu, B.; McNicholas, T. P.; Zhang, J.; Hilmer, A. J.; Jin, Z.; Reuel, N. F.; Kim, J.-H.; Yum, K.; Strano, M. S. *J. Am. Chem. Soc.* **2012**, *134*, 17620.

(17) Kim, J. H.; Ahn, J. H.; Barone, P. W.; Jin, H.; Zhang, J. Q.; Heller, D. A.; Strano, M. S. *Angew. Chem., Int. Ed.* **2010**, *49*, 1456.
(18) Ahn, J.-H.; Kim, J.-H.; Reuel, N. F.; Barone, P. W.; Boghossian, A. A.; Zhang, J.; Yoon, H.; Chang, A. C.; Hilmer, A. J.; Strano, M. S. *Nano Lett.* **2011**, *11*, 2743.
(19) Welsher, K.; Liu, Z.; Sherlock, S. P.; Robinson, J. T.; Chen, Z.; Daranciang, D.; Dai, H. J. *Nat. Nanotechnol.* **2009**, *4*, 773.
(20) Barone, P. W.; Yoon, H.; Ortiz-Garcia, R.; Zhang, J. Q.; Ahn, J. H.; Kim, J. H.; Strano, M. S. *ACS Nano* **2009**, *3*, 3869.
(21) Pfuetzner, S.; Meiss, J.; Petrich, A.; Riede, M.; Leo, K. *Appl. Phys. Lett.* **2009**, *94*, 223307.
(22) Strano, M. S.; Huffman, C. B.; Moore, V. C.; O'Connell, M. J.; Haroz, E. H.; Hubbard, J.; Miller, M.; Rialon, K.; Kittrell, C.; Ramesh, S.; Hauge, R. H.; Smalley, R. E. *J. Phys. Chem. B* **2003**, *107*, 6979.
(23) Dukovic, G.; White, B. E.; Zhou, Z. Y.; Wang, F.; Jockusch, S.; Steigerwald, M. L.; Heinz, T. F.; Friesner, R. A.; Turro, N. J.; Brus, L. E. *J. Am. Chem. Soc.* **2004**, *126*, 15269.
(24) Heller, D. A.; Jin, H.; Martinez, B. M.; Patel, D.; Miller, B. M.; Yeung, T. K.; Jena, P. V.; Hobartner, C.; Ha, T.; Silverman, S. K.; Strano, M. S. *Nat. Nanotechnol.* **2009**, *4*, 114.
(25) Choi, J. H.; Strano, M. S. *Appl. Phys. Lett.* **2007**, *90*, 223114.
(26) Wohlfarth, C. In *Landolt-Börnstein IV/17: Static Dielectric Constants of Pure Liquids and Binary Liquid Mixtures*; Lechner, M. D., Ed.; Springer-Verlag: Berlin Heidelberg, 2008; Vol. *17*.
(27) Fagan, J. A.; Zheng, M.; Rastogi, V.; Simpson, J. R.; Khripin, C. Y.; Silvera Batista, C. A.; Hight Walker, A. R. *ACS Nano* **2013**, *7*, 3373.
(28) Price, A. H.; Williams, J. O.; Munn, R. W. *Chem. Phys.* **1976**, *14*, 413.
(29) Ren, S. L.; Wang, Y.; Rao, A. M.; Mcrae, E.; Holden, J. M.; Hager, T.; Wang, K. A.; Lee, W. T.; Ni, H. F.; Selegue, J.; Eklund, P. C. *Appl. Phys. Lett.* **1991**, *59*, 2678.
(30) Ren, S. L.; Wang, K. A.; Zhou, P.; Wang, Y.; Rao, A. M.; Meier, M. S.; Selegue, J. P.; Eklund, P. C. *Appl. Phys. Lett.* **1992**, *61*, 124.
(31) Armbruster, J. F.; Roth, M.; Romberg, H. A.; Sing, M.; Schmidt, M.; Schweiss, P.; Adelmann, P.; Golden, M. S.; Fink, J.; Michel, R. H.; Rockenberger, J.; Hennrich, F.; Kappes, M. M. *Phys. Rev. B* **1994**, *50*, 4933.
(32) Moser, C. C.; Keske, J. M.; Warncke, K.; Farid, R. S.; Dutton, P. L. *Nature* **1992**, *355*, 796.
(33) Tanaka, Y.; Hirayama, K.; Niidome, Y.; Nakashima, N. *Chem. Phys. Lett.* **2009**, *482*, 114.
(34) Trasatti, S. *Pure Appl. Chem.* **1986**, *58*, 955.
(35) Ohkubo, K.; Imahori, H.; Shao, J. G.; Ou, Z. P.; Kadish, K. M.; Chen, Y. H.; Zheng, G.; Pandey, R. K.; Fujitsuka, M.; Ito, O.; Fukuzumi, S. *J. Phys. Chem. A* **2002**, *106*, 10991.
(36) Guldi, D. M.; Luo, C.; Kotov, N. A.; Ros, T. D.; Bosi, S.; Prato, M. *J. Phys. Chem. B* **2003**, *107*, 7293.
(37) Imahori, H.; Tamaki, K.; Guldi, D. M.; Luo, C.; Fujitsuka, M.; Ito, O.; Sakata, Y.; Fukuzumi, S. *J. Am. Chem. Soc.* **2001**, *123*, 2607.
(38) Imahori, H.; Tkachenko, N. V.; Vehmanen, V.; Tamaki, K.; Lemmetyinen, H.; Sakata, Y.; Fukuzumi, S. *J. Phys. Chem. A* **2001**, *105*, 1750.
(39) Henson, Z. B.; Welch, G. C.; van der Poll, T.; Bazan, G. C. *J. Am. Chem. Soc.* **2012**, *134*, 3766.
(40) Herranz, M. A.; Cox, C. T.; Echegoyen, L. *J. Org. Chem.* **2003**, *68*, 5009.
(41) Tamaki, K.; Imahori, H.; Nishimura, Y.; Yamazaki, I.; Shimomura, A.; Okada, T.; Sakata, Y. *Chem. Lett.* **1999**, *28*, 227.
(42) Allemand, P. M.; Koch, A.; Wudl, F.; Rubin, Y.; Diederich, F.; Alvarez, M. M.; Anz, S. J.; Whetten, R. L. *J. Am. Chem. Soc.* **1991**, *113*, 1050.
(43) Clarke, T. M.; Durrant, J. R. *Chem. Rev.* **2010**, *110*, 6736.
(44) Dresselhaus, M. S.; Dresselhaus, G.; Saito, R.; Jorio, A. *Annu. Rev. Phys. Chem.* **2007**, *58*, 719.